JOURNAL OF AIRCRAFT
Vol. 44, No. 5, September–October 2007

Analysis of Wind Tunnel Wall Interference Effects on Subsonic Unsteady Airfoil Flows

Karthikeyan Duraisamy*
University of Maryland, College Park, Maryland 20742
William J. McCroskey
U.S. Army Aeroflightdynamics Directorate, NASA Ames Research Center, Moffett Field, California 94035
and
James D. Baeder
University of Maryland, College Park, Maryland 20742

DOI: 10.2514/1.28143

In this work, the effect of wall interference on steady and oscillating airfoils in a subsonic wind tunnel is studied. A variety of approaches including linear theory, compressible inviscid and viscous computations, and experimental data are considered. Integral transform solutions of the linearized potential equations show an augmentation of the lift magnitude for steady flows when the wall is close to the airfoil surface. For oscillating airfoils, lift augmentation is accompanied by a significant change in the phase of the lift response. Idealized compressible Euler calculations are seen to corroborate the linear theory under conditions that are sufficiently away from acoustic resonance. Further, the theory compares well with compressible Reynolds-averaged Navier–Stokes calculations and experimental measurements over a wide range of attached flows at subsonic Mach numbers. The present methodology can thus be used to predict wall interference effects and also to help extrapolate linear and nonlinear (dynamic stall) wind tunnel data to free-air conditions.

Nomenclature

c	=	chord length
H	=	wall distance (in terms of semichord)
h/c	=	wall distance (in terms of c)
k	=	reduced frequency, $\frac{\omega c}{2U}$
M	=	freestream Mach number
U	=	freestream velocity
$w(x)$	=	downwash distribution (normalized by U)
x	=	chordwise distance
α	=	angle of attack, deg
β	=	Prandtl–Glauert factor, $\sqrt{1-M^2}$
$\Delta p(\xi)$	=	pressure difference between top and bottom (normalized by freestream dynamic pressure)
ξ	=	nondimensional distance along camber line
ϕ	=	phase angle between driving frequency and lift response
ω	=	angular velocity of pitching

Introduction

TYPICALLY, high Reynolds number experiments (of the order of 10^6 [1,2]) on airfoils are conducted in wind tunnel test sections that are not significantly larger than the model size. The proximity of the test section walls to the airfoil surface can be expected to affect the flowfield in a way that the measured forces cannot be directly extrapolated to free-flight conditions. Even though this is a relatively well-known fact, most computational fluid dynamics (CFD) simulations of wind tunnel experiments (for instance, [3,4]) are performed without modeling the tunnel wall.

In a steady attached flow around an airfoil, the primary effect of the wind tunnel wall is to present an effective blockage, thus resulting in an augmentation of lift. However, unsteady compressible flow (such as that corresponding to an oscillating airfoil) can be expected to be more complicated because of the fact that acoustic disturbances propagating from the airfoil surface reflect off the tunnel walls, and the resulting interaction can significantly affect the magnitude and phasing of the aerodynamic forces. For instance, Runyan and Watkins [5] demonstrate the possibility of succeeding disturbances reinforcing each other, causing an acoustic resonance. For a given tunnel height, this phenomenon occurs at a particular frequency of oscillation that is finite for all subsonic Mach numbers. Wind tunnel tests [6] showed a sharp reduction in the lift magnitude near the predicted frequency.

The broad objective of the present work is to characterize and predict the effect of wind tunnel wall interference on steady and oscillating airfoils. The following are the specific goals: 1) extensive study of the effects of wind tunnel interference on the lift response on an oscillating airfoil using linear theory, 2) assessment of the accuracy and validity of linear theory, 3) assessment of Euler and Reynolds-averaged Navier–Stokes (RANS) solvers in representing interference effects, and 4) investigation of the flowfield using Euler and RANS simulations.

Linear Theory

The problem of prediciting unsteady airloads on a thin airfoil has been investigated by a number of researchers over the past century. For the specific case of oscillating airfoils, major contributions were made by Theodorsen [7] and Possio [8]. Theodorsen derived an explicit expression for the force and moment on an oscillating flat plate in incompressible flow and expressed it in terms of Bessel functions. Possio obtained an integral equation relating the downwash and pressure distribution for subsonic compressible flow, which required a numerical solution. Whereas both of these approaches are valid for flow in an infinite domain, Bland's [9] work

Presented as Paper 2993 at the 24th AIAA Applied Aerodynamics Conference, San Francisco, 5–8 June 2006; received 8 October 2006; revision received 5 January 2007; accepted for publication 9 January 2007.

*Currently Department of Engineering, University of Glasgow, Glasgow, G12 8QQ Scotland, United Kingdom.

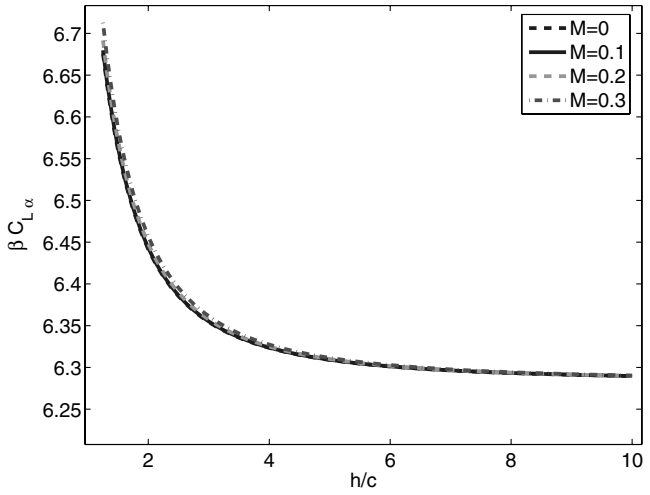

Fig. 1 Linear theory: Mach number corrected lift curve slope for steady flow over flat plate with varying Mach number and tunnel height.

appears to be the first to account for the presence of wind tunnel walls in subsonic compressible flow.

Based on an integral transform solution of the linearized full potential equation, this theory can be used to compute the surface pressure distribution Δp (and hence the forces), once the motion-induced downwash w on the airfoil is known. The solution involves a Fredholm integral equation of the first kind, given by

$$w(x) = \int_{-1}^{1} K(x-\xi)\Delta p(\xi)\,\mathrm{d}\xi \tag{1}$$

where the kernel function is given by

$$K(x) = \frac{\beta}{4\pi x} - \frac{ik}{4\pi}\log|x| + \frac{1+\operatorname{sgn}(x)}{8}k^2 e^{-ikx} - \frac{1}{4H}\left[\operatorname{sgn}(x)F'\left(\frac{|x|}{\beta H}\right) - \frac{ikH}{\beta}F\left(\frac{|x|}{\beta H}\right)\right]e^{\frac{ikM^2x}{\beta^2}} + \frac{1}{8H}\left[\operatorname{csch}\frac{\pi x}{2\beta H} - \frac{2\beta H}{\pi x} + (e^{\frac{ikM^2x}{\beta^2}} - 1)\operatorname{csch}\frac{\pi x}{2\beta H}\right] - \frac{ik}{4\pi\beta}\left[\log\left(\frac{1}{x}\tanh\frac{\pi x}{4\beta H}\right)\right] - \frac{ik}{4\pi\beta}\left[(e^{\frac{ikM^2x}{\beta^2}} - 1)\log\ \tanh\frac{\pi|x|}{4\beta H}\right]$$

where F and F' are functions (the latter being the derivative of the former) that can be summed up as an asymptotic series. The solution of this equation is obtained by collocation using a polynomial basis. The convergence properties and implementation details can be found in [10]. The method is very efficient in that only 6–10 collocation points are required to achieve convergence.

If the camber line (including the angle of attack) can be represented by the function $y(x)$, then the downwash function (in an oscillating case) is given by

$$w(x,t) = w(x)e^{i\omega t} = \left[\frac{\mathrm{d}}{\mathrm{d}x} + ik\right]y(x)e^{i\omega t} \tag{2}$$

It has to be mentioned that the preceding formulation reduces to well-known forms such as the Prandtl–Glauert solution for steady subsonic compressible flow and Theodorsen's theory for unsteady incompressible flow [7] under relevant simplifying assumptions. Rather surprisingly, this theory appears to have received relatively scant attention in the literature.

Figure 1 shows the effect of wall proximity on the lift curve slope of a flat plate in subsonic flow. It becomes clear that for wall heights $<3c$, significant lift augmentation can be expected. It is confirmed that for large h/c, the results asymptote to Glauert's result, $C_{L\alpha} = 2\pi/\beta$. Other than the Glauert correction, a weak dependence on Mach number is observed, except at very small h/c.

Figure 2 shows the amplitude $|C_{L\alpha}|$ and phase angle ϕ of the lift response for a flat plate oscillating (about the quarter-chord point and in incompressible flow) at different frequencies. As a measure of consistency, the results were verified to accurately compare with Theodorsen's theory for $h/c = \infty$. In addition, the distance of the wind tunnel walls from the airfoil surface is also varied. If the airfoil motion can be represented by $\alpha = \alpha_1\cos(\omega t)$, the lift response is given by $C_L(t) = \alpha_1|C_{L\alpha}|\cos(\phi + \omega t)$. It is evident that while lift augmentation occurs when the wall gets closer to the flat plate for a given frequency, the magnitude of the lift is reduced for increasing frequencies. In addition to the lift augmentation, the presence of the wall is seen to significantly determine the phasing. For instance, at $k = 0.175$, the presence of the wall for $1.25 < h/c < 4$ suggests a phase lag, whereas the freestream value corresponds to a clear phase lead. In general, the phase angle lags the forcing for small reduced frequencies and then leads for larger reduced frequencies, but this trend is delayed as the distance to the wind tunnel wall is smaller. It is also seen that the effect of the wind tunnel wall on the deviation of the phase angle (from free-air conditions) is larger for increasing frequencies.

As expected, Fig. 3 confirms the fact that compressible flow is much more complicated. As mentioned earlier, for particular combinations of the reduced frequency and wall distances, acoustic resonance between the oscillating (or driving frequency) and the waves reflected off the wind tunnel wall drastically alters the lift response. At such conditions, linear theory predicts infinite amplification. These *downwash independent* modes will be termed *Runyan modes* [5] and are related by

$$k_n = \frac{\pi\beta}{MH}\left(n - \frac{1}{2}\right), \qquad n = 0, 1, 2\ldots \tag{3}$$

Wind tunnel tests [6] confirm the existence of this phenomenon; however, damping in the form of nonlinearities and viscous effects diminish the exaggerated effect predicted by linear theory.

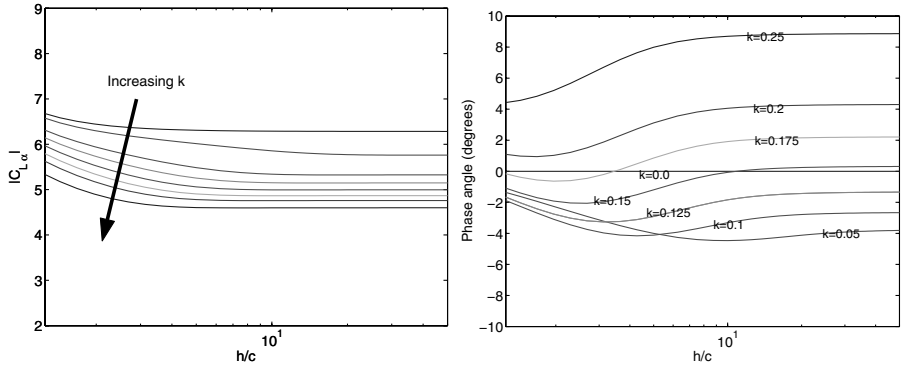

a) Amplitude of lift curve slope **b) Phase angle of lift response**

Fig. 2 Linear theory: lift slope and phase response for oscillating flat plate at $M = 0$ (incompressible flow).

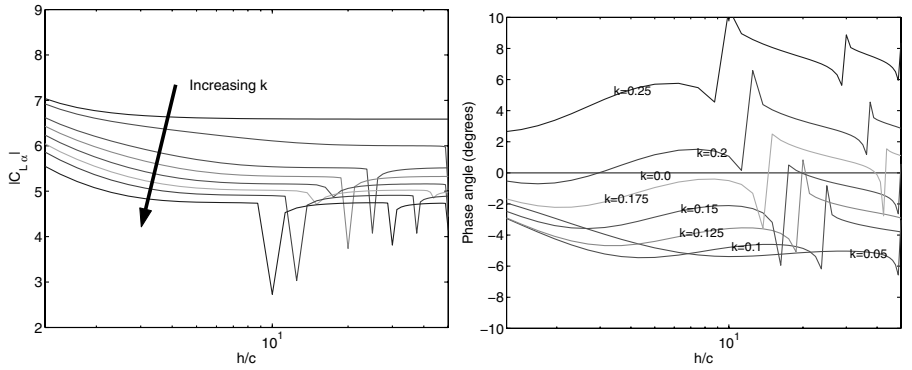

a) Amplitude of lift curve slope **b) Phase angle of lift response**

Fig. 3 Linear theory: lift slope and phase response for oscillating flat plate at $M = 0.3$ (subsonic compressible flow).

Numerical (CFD) Results

Computations are performed using a structured overset mesh solver. The compressible inviscid or RANS equations are solved using a high-order finite volume approach [11]. The inviscid terms are computed using the fifth-order weighted essentially non-oscillatory (WENO) [12] scheme with Roe's flux difference splitting [13]. The viscous terms are computed using fourth-order central differencing. Time integration is performed using the implicit second-order backwards difference scheme. The Spalart–Allmaras turbulence model [14] is used as a RANS closure when viscous results are sought. For the unsteady cases, dual time stepping is used with an appropriate number of subiterations to achieve 2–3 orders of magnitude of the L2 norm of the mean flow and turbulence model residuals. Typically, the attached flow cases required around 500 time steps per cycle for time converged results (to within plotting accuracy) and the dynamic stall calculation required around 1000 time steps per cycle. The dual time stepping is performed at a constant pseudo-Courant–Friedrichs–Lewy (CFL) number of 10 for the flow solver as well as the turbulence model.

A two-mesh system (as shown in Fig. 4) is used to discretize the flow domain. A body fitted C-mesh is used near the airfoil surface and this grid is overset inside a rectangular mesh that extends to the wind tunnel walls and the inflow and outflow boundaries. The airfoil mesh moves as a rigid body inside the static background mesh, thus ensuring a good mesh quality at all simulation times. The background mesh is hole-cut to blank out an extended region that encloses the airfoil surface. Subsonic characteristic inflow and outflow boundary conditions are specified at the left and right boundaries of the background mesh. On the wall surfaces (in both the background and airfoil meshes), density is extrapolated from the interior of the domain and the pressure is obtained from the normal momentum equation.

All the results presented in this work were verified to be grid- and time-step-converged. The grid-converged inviscid calculations are performed on a 201×61 (in the wraparound and normal directions, respectively) airfoil mesh, whereas the viscous calculations use a 317×121 mesh. The background mesh is made such that square cells of side $0.025c$ are used in the vicinity of the airfoil mesh. This yields 40 cells per chord length. Therefore, wavelengths of the order of $0.3c$ can be resolved satisfactorily by the numerical scheme. Note that the use of 500 time steps per cycle ensures that the time step is small enough to accurately represent the propagation of these waves. A typical background mesh size for $h/c = 2.5$ is 301×201 (in the streamwise and normal directions, respectively).

Inviscid Computations

For verification and validation purposes, the linear theory results are compared with inviscid computations on a NACA 0003 airfoil. This airfoil section was chosen because it roughly approximates the flat plate without singularities and acts a precursor for subsequent validation with experimental data on oscillating airfoils.

Figure 5 summarizes steady inviscid computations of the flow over a NACA 0003 airfoil. For each combination of M and h/c, the lift was computed for an angle of attack $\alpha = 1$ deg (and multiplied by $180/\pi$) to obtain the lift curve slope. For selected cases, an angle of attack sweep (from $-5 \leq \alpha \leq 5$ deg) was performed to confirm the linearity of the lift curve.

Figure 6 compares the computed lift response, for a sample oscillating NACA 0003 airfoil case, with linear theory. The angle of attack for these cases is given by $\alpha = 1 \sin(\omega t)$. The differences between the linear theory and CFD is observed to be within plotting accuracy. Figure 7 and Table 1 summarize the unsteady cases by comparing the magnitude and phasing of the first harmonic of the resultant lift curve slope.

In these cases, aside from the linearity assumptions in the theory, some differences can be expected from the geometric variations.

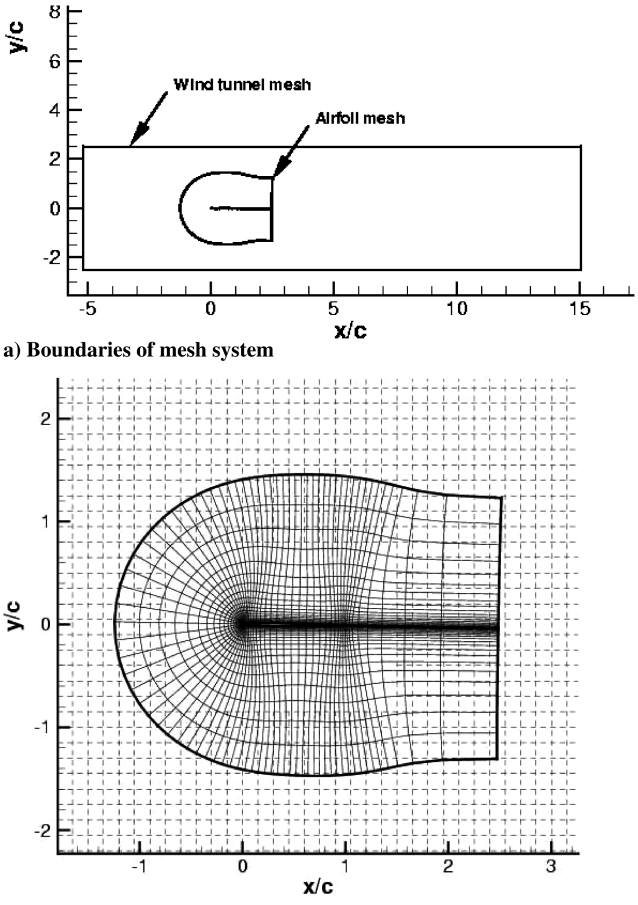

a) Boundaries of mesh system

b) Overlap and hole cut regions

Fig. 4 Sample mesh system for inviscid NACA 0003 computations.

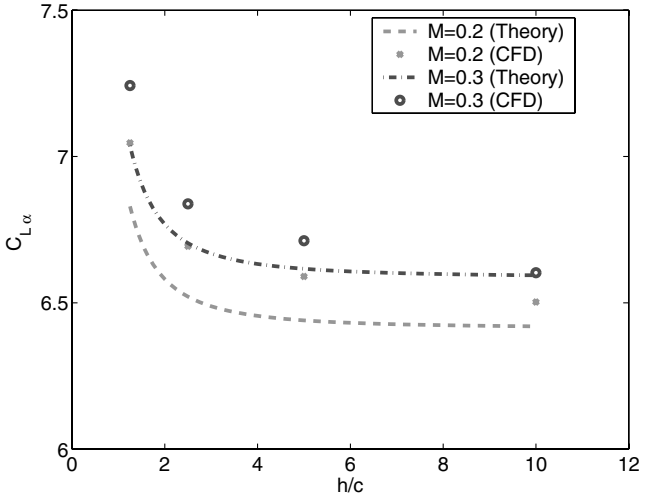

Fig. 5 Comparison between theory (flat plate) and inviscid computation (NACA 0003) for steady flow.

However, the level of agreement confirms the validity of the theory and also serves as a verification for the CFD computations.

Table 1 Comparison of first harmonic of lift response for NACA 0003 (inviscid computation) and flat plate (linear theory) at $M = 0.3$

h/c	k	$\lvert C_{L\alpha}\rvert_{\text{theory}}$	ϕ_{theory}	$\lvert C_{L\alpha}\rvert_{\text{Computed}}$	ϕ_{Computed}
1.25	0	7.037	0	7.242	0
2.50	0	6.703	0	6.838	0
5.00	0	6.616	0	6.712	0
10.0	0	6.594	0	6.602	0
1.25	0.05	6.920	−1.937	7.087	−2.578
2.5	0.05	6.505	−3.463	6.623	−3.809
5.0	0.05	6.284	−4.824	6.463	−4.541
10.0	0.05	6.108	−5.383	6.347	−4.794
1.25	0.1	6.618	−2.936	6.737	−3.468
2.5	0.1	6.049	−4.825	6.159	−5.050
5.0	0.1	5.697	−5.439	5.926	−6.017
10.0	0.1	5.538	−4.791	5.749	−6.371
1.25	0.15	6.234	−2.479	6.316	−2.719
2.5	0.15	5.569	−3.576	5.668	−3.788
5.0	0.15	5.237	−2.847	5.394	−4.408
10.0	0.15	5.161	−2.103	5.199	−3.658
1.25	0.2	5.859	−0.529	5.933	−0.383
2.5	0.2	5.187	−0.344	5.277	−0.583
5.0	0.2	4.939	1.164	4.996	−0.584
10.0	0.2	4.902	1.068	4.871	0.190

Validity of Linear Theory Near Resonance Conditions

As observed in Fig. 6, the comparison between linear theory and inviscid CFD prove to be good for the conditions that were evaluated. The validity of the linear theory will now be examined at a higher Mach number near resonance conditions. Figure 8 shows the amplitude and phasing of the lift response at $M = 0.5$. As a representative case, $h/c = 5.0$ will be considered, and for this case, acoustic resonance occurs near $k = 0.25$. Figure 9 compares the linear theory with inviscid calculations and it is evident that near resonance, the discrepancy in both the amplitude and phasing is substantial. This can be attributed to the damping introduced by the nonlinear interactions. Figure 10 shows the "perturbation" pressure coefficient (instantaneous pressure with a subtract of the pressure corresponding to steady flow at mean α) at a sample time. The complicated interaction of a circular acoustic pulse (in the figure, centered at $\{x, y\} \approx \{3, 0\}$ and of radius ≈ 3 with waves reflecting off the wall) is evident. It has to be mentioned that the computed solution may not be entirely physical because 2-D acoustic propagation is essentially different compared to the 3-D problem.

Validations with Experimental Data

To validate the linear theory and the CFD methodology with experiments, comparison with oscillating NACA 0012 data from the U.S. Army Mobility Research and Development Laboratory (AMRDL)-Ames 7 × 10 ft subsonic wind tunnel [1,2] is attempted.

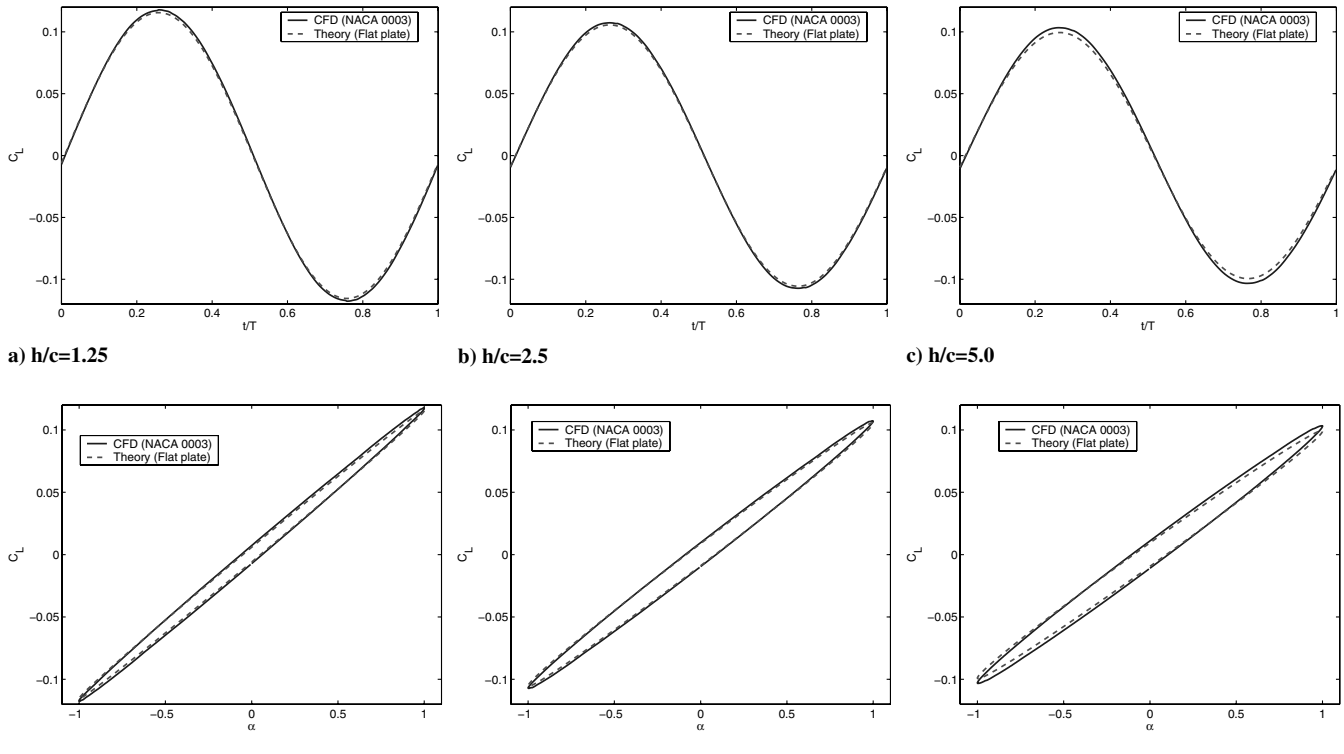

a) h/c=1.25 **b) h/c=2.5** **c) h/c=5.0**

d) h/c=1.25 **e) h/c=2.5** **f) h/c=5.0**

Fig. 6 Comparison of lift response for oscillating NACA 0003 (inviscid computation) and flat plate (linear theory) at $M = 0.3, \alpha = 1\sin(2kMt), k = 0.1$: a), b), c) vs time; d), e), f) vs α.

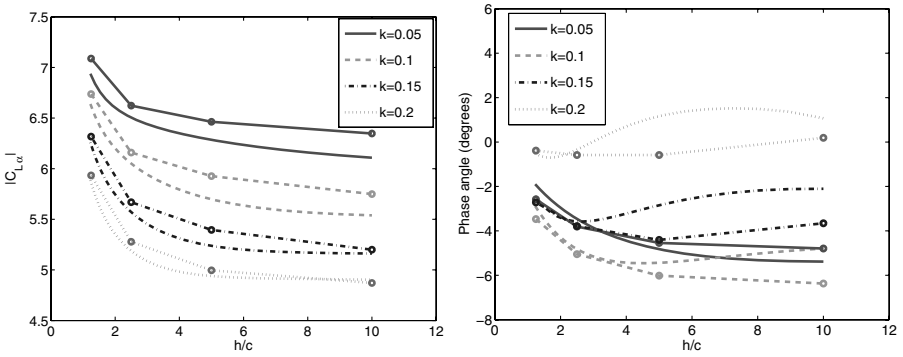

a) Lift curve slope **b) Phase angle**

Fig. 7 Comparison of first harmonic of lift response for oscillating NACA 0003 (inviscid computation, lines + symbols) and flat plate (linear theory, lines) at $M = 0.3$.

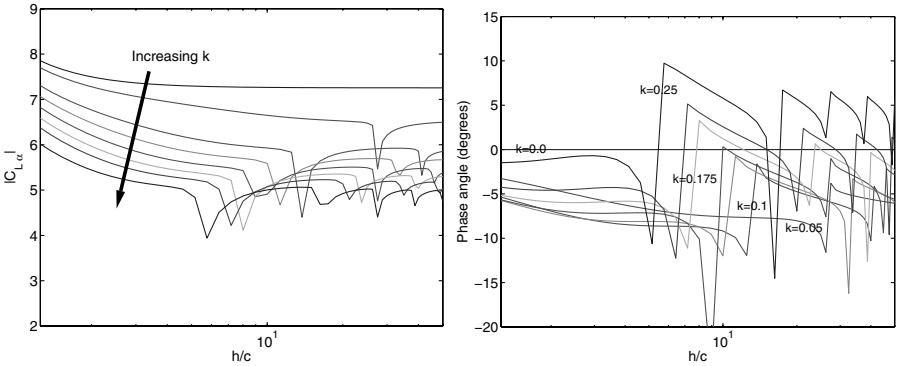

a) Amplitude of lift curve slope **b) Phase angle of lift response**

Fig. 8 Linear theory: lift slope and phase response for oscillating flat plate at $M = 0.5$, $h/c = 0.5$.

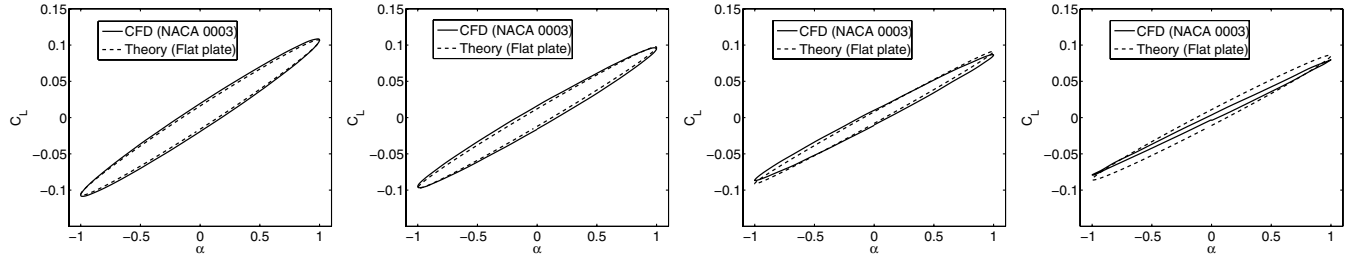

a) k=0.1 **b) k=0.15** **c) k=0.2** **d) k=0.25**

Fig. 9 Comparison of lift response for oscillating NACA 0003 (inviscid computation) and flat plate (linear theory) at $M = 0.5$, $\alpha = 1\sin(2kMt)$.

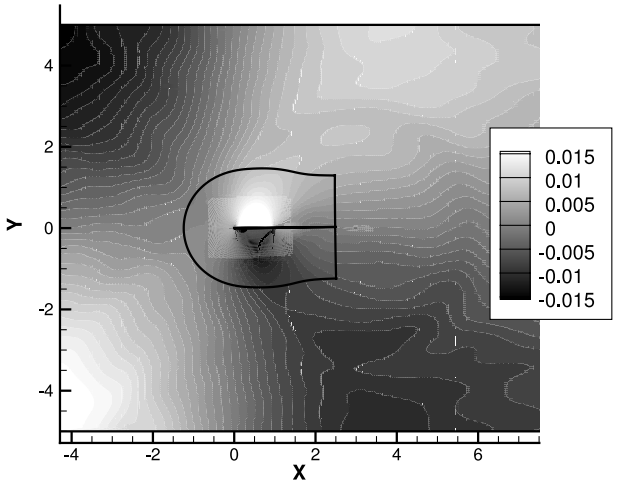

Fig. 10 Contours of perturbation pressure coefficient for NACA 0003 at $M = 0.5$, $k = 0.25$, $t/T = 0.6$.

A set of test cases are shown in Table 2. This set was chosen because it represents an effective frequency sweep at attached flow conditions. Figure 11 compares the linear theory and RANS computations for the aforementioned cases. In these cases, even though thickness effects can be expected to be more prominent than in the NACA 0003 cases, the overall agreement of the linear theory with experiments and computations is good. The computed pressure distributions (for a sample case, case 2) are shown in Fig. 12 and the level of agreement effectively validates the RANS solver.

Table 2 Experimental test cases for validation of oscillating NACA 0012 airfoil data with linear theory and RANS computations: $\omega = 2kM$

Case	h/c	k	α, deg	M	Re	Reference
1	2.5	0.01	$4.95 + 5\sin(\omega t)$	0.3	3.93×10^6	[2]
2	2.5	0.1	$4.95 + 5\sin(\omega t)$	0.3	3.93×10^6	[2]
3	1.25	0.15	$6 + 6\sin(\omega t)$	0.1	2.5×10^6	[1]
4	1.25	0.24	$6 + 6\sin(\omega t)$	0.1	2.5×10^6	[1]

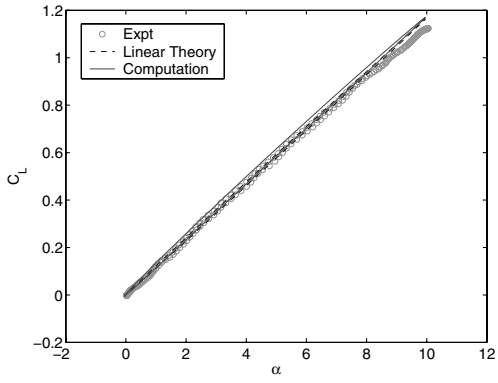

a) Case 1 (k = 0.01)

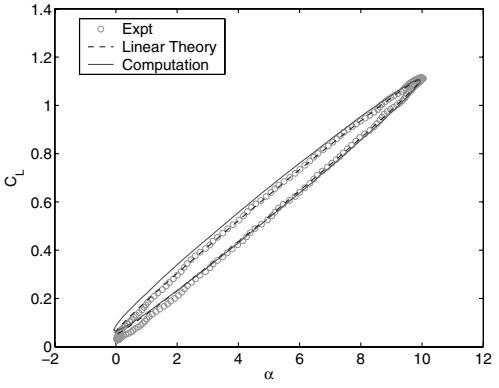

b) Case 2 (k = 0.1)

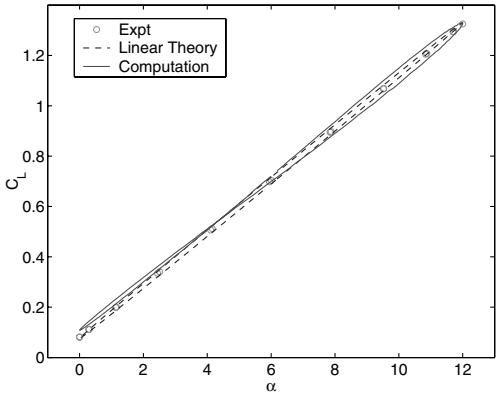

c) Case 3 (k = 0.15)

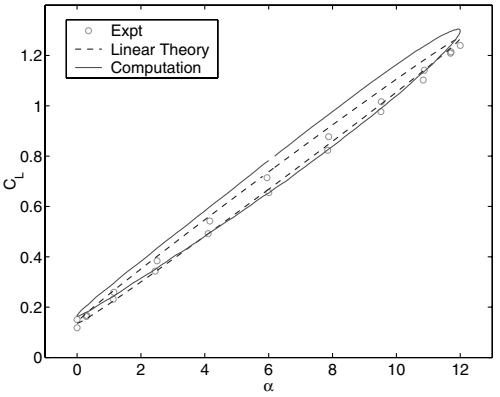

d) Case 4 (k = 0.24)

Fig. 11 Comparison of lift response for several NACA 0012 configurations. Refer to Table 2 for further details.

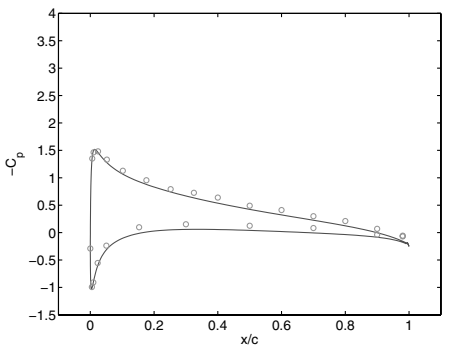

a) α = 4.94°, t/T = 0

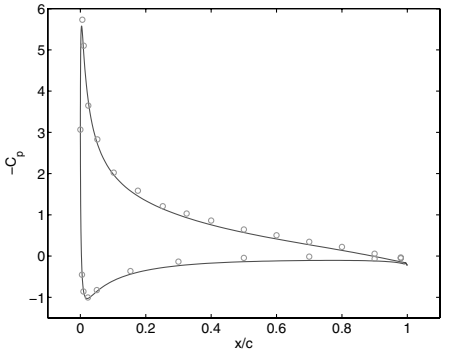

b) α = 9.94°, t/T = 0.25

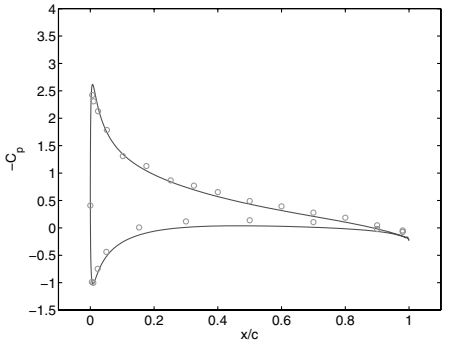

c) α = 4.94°, t/T = 0.5

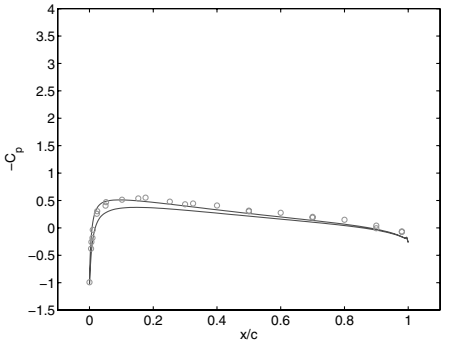

d) α = −0.06°, t/T = 0.75

Fig. 12 Case 2: surface pressure distribution.

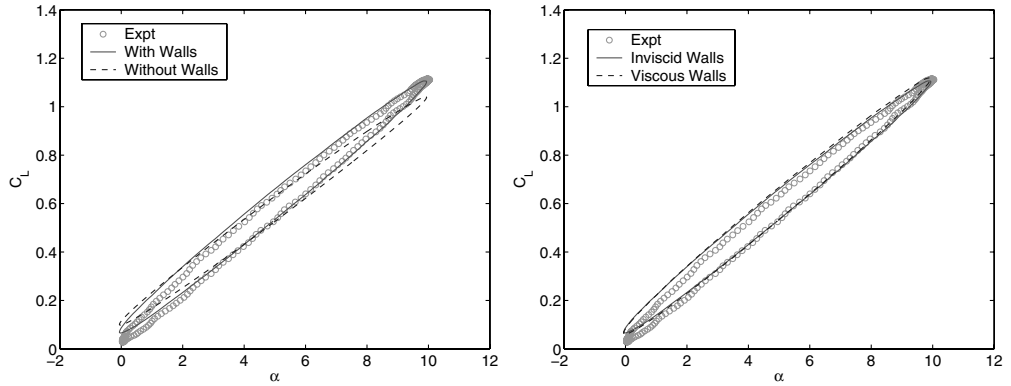

a) Effect of inclusion of wind tunnel wall

b) Effect of type of wind tunnel wall boundary condition

Fig. 13 Case 2: effect of wind tunnel wall.

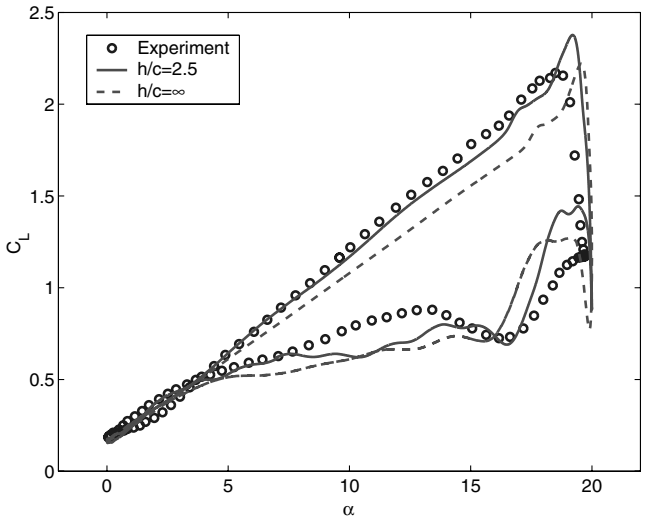

Fig. 14 Lift response of SC1095 airfoil undergoing dynamic stall at $M = 0.302, k = 0.099$.

Figure 13 further confirms the fact that inclusion of the wind tunnel walls significantly affects the computed lift curve slope. However, as expected from Fig. 3, the difference in phase angle for this combination of M and k is not considerably different for $h/c = 2.5$ and $h/c = \infty$.

Impact on Dynamic Stall Calculations

For practical implications of the aforementioned interference effects (and also to validate the numerical algorithm under separated flow conditions), a dynamic stall simulation is considered. The experiment [2] corresponds to an SC1095 airfoil at $M = 0.302$, $Re = 3.92 \times 10^6$, $k = 0.099$, oscillating at an angle of attack given by $\alpha = 9.78 + 9.9 \sin(\omega t)$. The wind tunnel walls are at a distance of $2.5c$ from the airfoil surface. As seen from Fig. 14, inclusion of wind tunnel walls in the computation significantly improves the prediction of the lift response on the upstroke. Investigation of the flowfield data showed that at the tunnel walls, the variation of the pressure coefficient ranged between ± 0.3 and remained significant up to five chords upstream and downstream of the airfoil.

Conclusions

The proximity of the wall has significant effects on the forces acting on steady and oscillating airfoils in wind tunnels. In this work, Bland's [9] integral transform solution of the linearized compressible potential equations was examined for steady and oscillating airfoils over a wide range of tunnel heights and frequencies. Analysis of the solutions suggest the following:

1) For steady flow, there is significant lift augmentation (compared to a freestream test) at wall distances approximately less than three chords from the airfoil surface.

2) For unsteady flow, whereas the effect on the magnitude of the lift curve slope is again significant for wall distances less than three chords from the airfoil surface, the phasing is significantly affected at *all wall distances* for compressible flow. The effect of the wind tunnel wall on the deviation of the phase angle (from free-air conditions) is, in general, larger for increasing frequencies. The lift response is drastically altered near conditions corresponding to acoustic resonance between the airfoil and wind tunnel walls.

The theoretical results were validated with compressible Euler calculations. The level of agreement of the predicted lift response with theory was found to be very high for conditions that are not near the acoustic resonance. Linear theory and RANS calculations also compare well with experimental data corresponding to subsonic high Reynolds number attached flow at various oscillating frequencies. For all the test cases, the importance of accounting for the wind tunnel wall is clearly established.

The aforementioned tests confirm the validity of the linear theory as a low-cost tool for interpreting oscillating airfoil wind tunnel data and extrapolating the same to freestream conditions. In addition, the RANS methodology also proves to be a reliable predictive means to study unsteady compressible flows in the presence of interfering wind tunnel walls.

Acknowledgments

This work is sponsored by Defense Advanced Research Projects Agency (DARPA) under U.S. Army Research Office Contract No. W911NF-04-C-0102. The authors would like to thank the DARPA project review team for their encouragement and support.

References

[1] McAlister, K. W., Carr, L. W., and McCroskey, W. J., "Dynamic Stall Experiments on the NACA 0012 Airfoil," NASA Technical Paper 1100, 1978.

[2] McAlister, K. W., Pucci, S. L., McCroskey, W. J., and Carr, L. W., "An Experimental Study of Dynamic Stall on Advanced Airfoil Sections," Vol. 2, NASA Technical Memorandum 84245, 1982.

[3] Martin, P. B., McAlister, K. W., Chandrasekhara, M. S., and Geissler, W., "Dynamic Stall Measurements and Computations for a VR-12 Airfoil with a Variable Droop Leading Edge," *59th Annual Forum of the American Helicopter Society Proceedings* [CD-ROM], American Helicopter Society, Phoenix, AZ, 2003.

[4] Datta, A., and Chopra, I., "Prediction of UH-60A Dynamic Stall Loads in High Altitude Level Flight Using CFD/CSD Coupling," *61st Annual Forum of the American Helicopter Society Proceedings* [CD-ROM], American Helicopter Society, Grapevine, TX, 2005.

[5] Runyan, H. L., and Watkins, C. E., "Considerations on the Effect of Wind Tunnel Walls on Oscillation Air Forces for Two Dimensional Subsonic Compressible Flow," NACA Report 1150, 1953.

[6] Runyan, H. L., Woolston, D. S., and Rainey, A. G., "Theoretical and

Experimental Investigation of the Effect of Tunnel Walls on the Forces on an Oscillating Airfoil in Two Dimensional Subsonic Compressible Flow," NACA Report 1262, 1956.

[7] Theodorsen, T., "General Theory of Aerodynamic Instability and the Mechanism of Flutter," NACA Report 496, 1935.

[8] Possio, C., "L'azione Aerodinamica sul Profilo Oscillante in un Fluido Compressible a Velocita Iposonora," *L'Aerotechnica*, Vol. 18, No. 4, 1938, pp. 421–458.

[9] Bland, S. R., "The Two Dimensional Oscillating Airfoil in a Wind Tunnel in Subsonic Flow," *SIAM Journal on Applied Mathematics*, Vol. 18, No. 4, 1970, pp. 830–848.

[10] Fromme, J., and Goldberg, M., "Unsteady Two Dimensional Airloads Acting on Oscillating Thin Airfoils in Subsonic Ventilated Wind Tunnels," NASA Contractor Report 2987, 1978.

[11] Duraisamy, K., "Studies in Tip Vortex Formation, Evolution and Control," Ph.D. Dissertation, Dept. of Aerospace Engineering, Univ. of Maryland, College Park, MD, 2005.

[12] Shu, C.-W., "High-Order Finite Difference and Finite Volume WENO Schemes and Discontinuous Galerkin Methods for CFD," *International Journal of Computational Fluid Dynamics*, Vol. 17, No. 2, 2003, pp. 107–118.

[13] Roe, P., "Approximate Riemann Solvers, Parameter Vectors and Difference Schemes," *Journal of Computational Physics*, Vol. 43, 1981, pp. 357–372.

[14] Spalart, P. R., and Allmaras, S. R., "A One-Equation Turbulence Model for Aerodynamic Flows," AIAA Paper 92-0439, June 1992.